# *INTEGRAL*

## *Announcement of Opportunity for Observing Proposals (AO-3)*

# SPI Observer's Manual

Written by: T. Oosterbroek

Integral Science Operations, ESTEC

based upon inputs from:
J.P. Roques, SPI Co-PI, CESR Toulouse
V. Schönfelder, SPI Co-PI, MPE Garching
P. Jean, SPI-CoI, CESR Toulouse.

13 September 2004
Issue 3

Ref. nr. INT-SOC-DOC-022

This page was intentionally left blank

# Table of Contents


I. Introduction . . . . . 5
II. Description of the instrument . . . . . 6
1. Overall design . . . . . 6
2. The Passive Mask . . . . . 7
3. The Camera . . . . . 8
3.1 Cryostat . . . . . 8
3.2 Detectors and pre-amplifiers . . . . . 9
3.3 The detector electronics . . . . . 9
3.4 Pulse shape discriminator (PSD) . . . . . 9
4. Anti-Coincidence Subassembly (ACS) . . . . . 10
5. The Plastic Scintillator Anti Coincidence Subassembly (PSAC) . . . . 10
6. Electronics . . . . . 10
III. Instrument Operations . . . . . 12
1. How the instrument works. . . . . 12
2. Operating modes . . . . . 12
3. Dead time . . . . . 13
4. Telemetry budget . . . . . 13
IV. Using the instrument . . . . . 14
1. Spectroscopy and timing . . . . . 14
2. Imaging . . . . . 15
3. Gamma-ray burst detection . . . . . 15
V. Performance of the instrument . . . . . 17
1. Components and sources of instrumental background . . . . . 17
1.1 Continuum background . . . . . 17
1.2 511 keV background . . . . . 17
1.3 Background gamma-ray lines . . . . . 18
2. Instrumental characterisation and calibration . . . . . 19
3. Measured performance . . . . . 19
3.1 Imaging resolution . . . . . 19
3.2 Spectral resolution . . . . . 20
3.3 Dithering sensitivity degradation . . . . . 25
3.4 Detection of off-axis sources . . . . . 26
3.5 Imaging capabilities . . . . . 26
3.6 Timing capabilities . . . . . 28
VI. Observation "Cook book" . . . . . 30
1. Astronomical considerations on the use of the instrument . . . . . 30
2. How to estimate observing times . . . . . 30
2.1 Gamma-ray line . . . . . 31
2.2 Gamma-ray continuum . . . . . 31
3. Worked examples . . . . . 32

This page was intentionally left blank

# I. Introduction

This document is meant to tell the observers what the SPI instrument is, how it works and how to use it for astronomical observations.

The INTEGRAL payload consists of four instruments, two gamma ray instruments (a spectrometer, SPI, and an imager, IBIS) and two monitoring cameras (an X-ray monitor, JEM-X, and an optical monitor, OMC). Whereas the main scientific goal for the IBIS instrument is high resolution imaging of gamma ray sources with some spectroscopic capabilities, the scientific goal for the SPI (Spectrometer onboard INTEGRAL) instrument is high resolution gamma ray spectroscopy with some imaging capabilities in the 20 to 8000 keV range. The SPI instrument is the first high resolution gamma ray spectral imager to operate in this energy range. SPI is the next major breakthrough in the field of gamma ray spectroscopy and nuclear astrophysics after the highly successful Compton Gamma Ray Observatory (CGRO).

The spectrometer SPI has been developed for ESA under the responsibility of CNES, Toulouse as prime contractor. Subsystems for SPI have been built by: DARA and MPE (Germany; Anti-coincidence subsystem), the University of Louvain (Belgium; Germanium for detectors), CESR (France; Ge detectors and their electronics), CEA (France; Digital Front End Electronics), CNES (France; cryostat, lower structure, flight software, thermal control), University of Valencia (Spain; coded mask), IFCTR Milano (Italy; Plastic Scintillator) and the University of Berkeley and San Diego (USA; Pulse Shape Discriminator). The instrument has two Co-PIs: J.P. Roques (CESR, Toulouse, France) and V. Schönfelder (MPE, Garching, Germany). Later this year R. Diehl (MPE, Garching) will replace V. Schönfelder.

# II. Description of the instrument

## 1. Overall design

The SPI instrument design is based on a hexagonal geometry, which is the most compact one. The instrument is a coded mask spectrometer. The main characteristics of the instrument are given in Table 1. An overall cut-out view of the instrument is given in Figure 1.

**Table 1 Main characteristics of the SPI instrument.**

| | |
|---|---|
| Mask dimensions | 665 mm flat to flat<br>30 mm thick Tungsten |
| Detector unit | Encapsulated Ge, hexagonal geometry, 19 detectors<br>70 mm thick |
| Energy range | 18 keV - 8 MeV |
| Energy resolution (FWHM) | 2.2 keV at 1.33 MeV for each detector, 3 keV for the whole spectrometer. |
| Angular resolution | $2.5^o$ for point sources |
| Point source positioning | $<1.3^o$ for point sources (depending on point source intensity) |
| Field-of-View | fully coded: $13.2^o$ flat to flat,<br>$16^o$ corner to corner<br>zero coding: $30.5^o$ flat to flat,<br>$35^o$ corner to corner (zero sensitivity) |

The detector of the instrument consists of 19 cooled, hexagonally shaped, high purity Ge detectors, providing a total area of about 500 $cm^2$. The background on the detectors is limited by use of several methods. A Pulse Shape Discriminator system (PSD) reduces the $\beta$ decay background in the Ge. An Anti-Coincidence veto System (ACS), consisting of 91 bismuth-germanate (BGO) scintillator blocks vetos out-of-field photons and particles, and a plastic scintillator underneath the coded mask vetos photons originating in the mask. The veto shield also defines the field-of-view of the instrument, since it vetoes the out-of-field photons. The sensitivity of the instrument is limited by the background due to the primary and secondary cosmic ray particles and the cosmic background radiation.

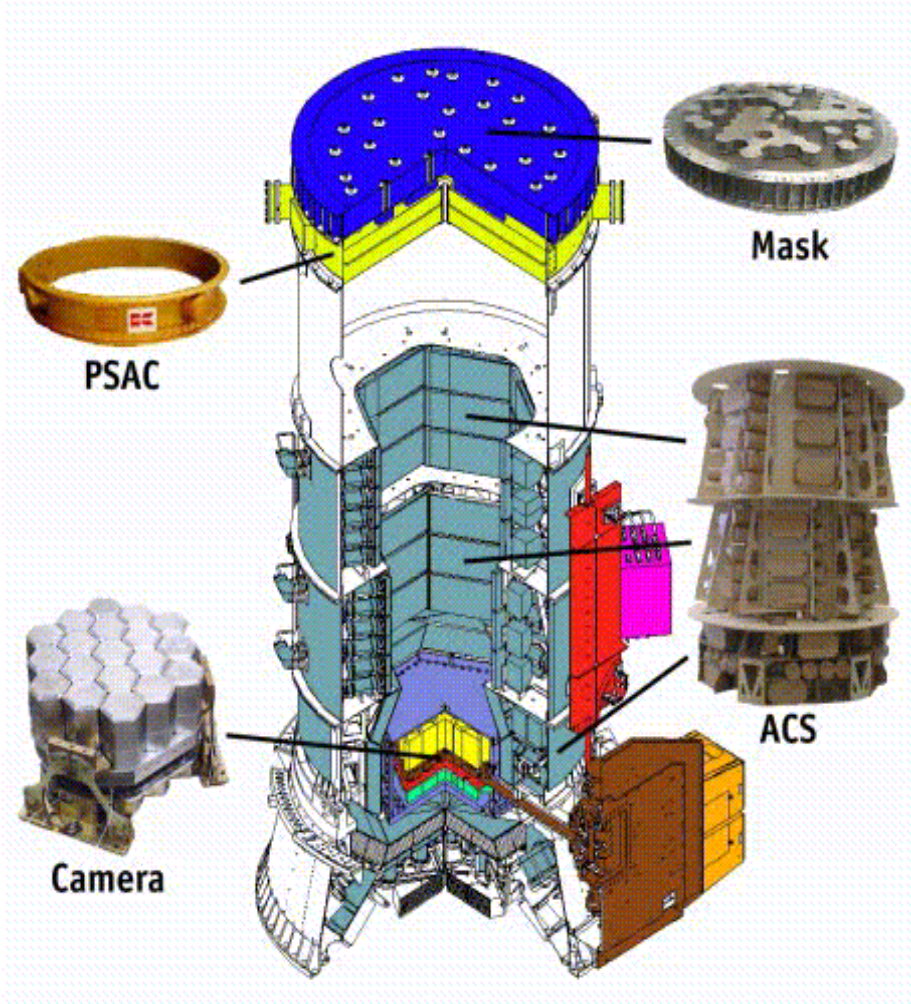


**Figure 1 A cut-away view of the SPI instrument. The mask, plastic scintillator, camera and ACS subsystems are highlighted.**

## 2. The Passive Mask

The passive mask is located at the top of the SPI instrument, above the plastic scintillator. The purpose of the mask is to code the incident gamma rays in the field-of-view, giving the instrument imaging capabilities. The mask also provides stiffness to the primary structure of the SPI instrument.

The mask consists of a sandwich structure made of:

- a nomex honeycomb core covered by two skins,
- a titanium ring that forms the interface to the rest of the instrument
- a coded motif made of hexagonal tungsten blocks that are stuck and screwed onto the sandwich structure.

The tungsten motif provides the specific transparency and geometry for the mask. The mask is made of 127 elements of hexagonal shape and inscribed in a 78 cm diameter circle. Of these elements 63 are opaque and 64 are transparent. Each opaque element is 30 mm thick and 60 mm flat to flat in size. The tungsten elements stop the gamma ray radiation in the range 20 keV to 8 MeV with an absorption efficiency greater than 95% at 1 MeV. The holes in the mask have a gamma ray transparency of 60% at 20 keV and 80% at 50 keV. The mask is located 171 cm from the detector plane. The distance between the mask and the detector plane is driven by the required field-of-view and angular resolution. The total mass for the mask is 139.4 kg (10 kg titanium, 107 kg tungsten, rest in other materials). A picture of the mask pattern is given in Figure 2

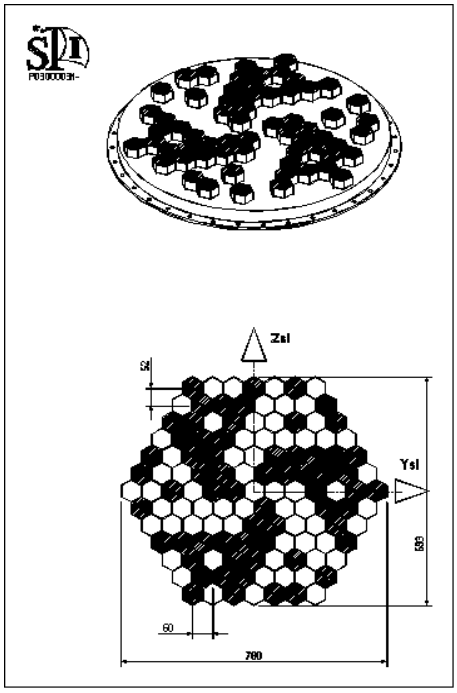


**Figure 2 The passive mask of the SPI instrument. The bottom picture indicates the direction of the spacecraft Y and Z axes with respect to the mask. (See the *"INTEGRAL Manual"* for the definitions of the axes.)**

# 3. The Camera

## 3.1 Cryostat

For an optimum sensitivity and resolution the detectors of the SPI instrument have to be kept at a constant, low temperature of 85 K. The SPI cryostat (which is made in Be) is designed to keep

the detectors at this optimum operating temperature. The cryostat is composed of three parts: an active cooling system, a passive cooling system and a cold box. The active cooling system brings the temperature of the cold plate on which the detectors are mounted down to 85 K, using two pairs of cryocoolers. In normal operating mode all coolers work simultaneously. In case of failure of one of the cryocoolers, or of the electronics, the instrument will be functional, but in a degraded mode, as the detector temperature can rise to more than 100 K. The detector assembly is placed inside the cold box, which is kept at approximately 210 K by the passive cooling system. All temperatures of the cryostat subsystems are regularly monitored to provide the ground operators with early warnings on failures of coolers, and to provide temperature information that can be used for the data processing.

### 3.2 Detectors and pre-amplifiers

The detectors used for SPI are 19 hexagonal-shaped Be encapsulated high purity Germanium detectors, mounted on a cold plate at 85 K, as close as possible together. The size of the detectors is 5.6 cm, flat to flat, with a height of 7 cm. The cold plate is made of beryllium and it is directly cooled by the SPI cooling system. The bottom of the cold plate is hollowed to mount the printed board pre amplifiers (PA-1) cold electronics. The PA-1 electronics include the high voltage filter and the connection between the detector and the Charge Sensitive Amplifier (CSA). A second set of 19 pre-amplifiers (PA-2) is mounted on a second cold plate (beryllium, at 210 K). The PA-2 is connected to the PA-1 with a cryogenic cable.

The hexagonal detectors are mounted with minimum space between them, such that the axes of two adjacent detectors are 6 cm apart. The material in front of the detector has good transparency for gamma-rays at 20 keV. To cure the degeneration of the Ge detectors, an annealing operation is performed approximately every 6 to 12 months, strongly, in which the detectors are heated to 105 degrees C. The instrument will not be available for scientific observations during the time needed for the annealing operation and the cooling phase afterwards (in total 4 revolutions, equivalent to 12 days).

### 3.3 The detector electronics

The signals from the pre-amplifiers are sent to the amplification chain, which is made up of a Pulse Shape Amplifier (PSA) and a Pulse Height Amplifier (PHA). The PSA amplifies the pulses such that the performance of the spectrometer is optimised. This is done by making a compromise between getting the best signal to noise ratio for the pulses, operating in the full 20 keV-8 MeV energy band of the instrument without resolution degradation, and making the output pulses insensitive to the fluctuations in the detector signal rise time. The PHA is used to maintain the energy resolution in the full 20 keV-2 MeV or 2 MeV to 8 MeV range. Finally the detector electronics also comprise a high voltage power supply (0-5000 V) and a low voltage power supply (19 independent chains per amplification chain).

### 3.4 Pulse shape discriminator (PSD)

The PSD subsystem compares the form of the pulses produced by the pre amplifiers with profiles stored in an onboard archive. Based on this comparison the PSD flags each event with a signal type (single or multiple event), and consequently the type of processing necessary. Only non-vetoed events are processed by the PSD. The output of the PSD is provided to the Data Processing Electronics (DPE, see below). The PSD works in an energy range from 200 keV to 1 MeV. The

onboard pulse shape library is verified twice a year in connection with the annealing of the detectors. The PSD is important to identify the background photons impacting on the detector. It reduces the background between 200 keV and 1 MeV by, and thus increases the sensitivity of the instrument in this energy range..

## 4. Anti-Coincidence Subassembly (ACS)

The main function of the Anti-Coincidence Subassembly (ACS) is to shield the Ge detectors against background (photons and particles) from sources outside the field-of-view. The ACS system consists of 91 Bismuth Germanate (BGO) scintillator crystals in combination with photo multiplier tubes. The BGO crystal thickness has been optimised with Monte Carlo simulations to minimize the detector background (by minimizing the shield leakage and neutron induced radiation in the BGO). The BGO shield for the side and the rear of the camera is 5 cm thick. The complete shield consists of two collimator rings (that define the SPI field-of-view), located between the mask and the camera unit, a side shield and a rear shield that surround the camera. The BGO scintillator crystals are used to convert all incoming events into photons in the 480 nm region (visible light). Photo-multiplier tubes are used to detect these photons and convert them into electrical pulses which are sorted, normalised and summed up by the ACS electronics. Each photon induces a time tagged veto signal. The ACS output data is directed to the Digital Front End Electronics (DFEE) which formats the data and time tags each event. Photons that are not in coincidence with an ACS veto event are considered "good". The ACS-off photons (i.e all photons that are detected by the Ge detectors, independent of the veto status) are integrated into background spectra, that are sent to the ground every 30 minutes.

## 5. The Plastic Scintillator Anti Coincidence Subassembly (PSAC)

The purpose of the plastic scintillator subassembly (PSAC) is to reduce the 511 keV background due to particle emission by the passive mask. The detector consists of a plastic scintillator inside a light tight box, located just below the passive mask. It has a good gamma ray transparency, and actively detects particles which deposit energies in excess of 300 keV. The light flashes that are produced by the impacts of these high energy particles are detected with four photo multiplier tubes located around the light-tight box and converted into electrical pulses which are processed by the PSAC electronics assembly. The electronics send a veto signal associated with the detected events and compatible with the Anti-Coincidence Subassembly (ACS) Front End electronics veto signal to the veto control unit of the ACS.

## 6. Electronics

The electronics is divided into the Digital Front End Electronics (DFEE) and the Data Processing Electronics (DPE). The DFEE is in charge of the real time acquisition, assembly, time

stamping and intermediate storage of the various pieces of information coming from the SPI front end systems (detector electronics, PSD, ACS etc.). The DFEE subdivides the events into classes depending on their origin in the instrument (detector electronics, Ge detectors, PSD, veto shield) and handles overall event energies and system monitoring statistics (dead time, signal counts etc.). The detected events are time tagged with a 20 MHz local clock, which provides the timing resolution. The reset (timing reference) is done with the 8 Hz satellite clock. The DFEE uses the 125 ms time frames to analyse and process the input information and pass it on to the DPE. The statistics are passed on to the DPE every second. The DPE is the interface to the instrument. It is part of the On Board Data Handling (OBDH) unit. It provides the telecommand and telemetry interfaces to the instrument and it provides the environment for the instrument dedicated software (Instrument Application Software, IASW).

# III. Instrument Operations

## 1. How the instrument works.

The SPI instrument provides a combination of high-resolution spectroscopy with imaging capabilities. The performance characteristics of the instrument each depend on one of the instrumental subsystems:

- Energy resolution: is determined by the cooled Ge detectors
- Angular resolution: is determined by the pixel size of the mask and the detector and the distance between them. However imaging with SPI requires a special operation (dither) since a single pointing does not unambiguously define a sky image. For this the 5 by 5 and hexagonal dithers have to be used (see below).
- Field-of-View: determined by the area of the mask and the detector and the distance between them, as well as the ACS shield.
- Sensitivity: achieved by making the detector as large as possible and by minimizing the background (by using an ACS that is optimised in material and thickness, by incorporating a PSD system, by carefully choosing the materials used in the instrument and by adding a plastic scintillator below the mask).

The passive mask provides the shadowgram for image reconstruction. The PSAC detects energetic particles originating in the mask, and provokes a veto pulse from the veto system. The ACS detects gamma rays and charged particles from out of field sources, and also provokes a veto pulse. Each photon that is absorbed in a Ge detector will give a pulse that is sent to the electronics. The electronics analyses the incoming pulses and the veto signals and tags each photon with the energy, the time and the type of event (i.e. single detector events with or without PSD and multiple detector events). These data are then sent to the ground (see below). The ACS-off photons are summed into background spectra, that are sent to the ground every 30-60 minutes.

## 2. Operating modes

The SPI instrument has only one mode for normal observations. All scientific observations with SPI are done in a so called photon by photon mode with a high temporal resolution. In this mode scientific data is collected and transmitted to the ground for each photon. However, due to telemetry limitations, only certain types of detected photons are transmitted directly; the rest is in the detector spectra. For each detected photon, data is sent to the ground from which the type of event, the energy and the timing can be deduced. Furthermore detector spectra of all events (including vetoed events) can be accumulated and transmitted every 30-60 minutes. However, currently these spectra are not transmitted, which means in the case of telemetry overflow a loss of events. It is likely that the spectral accumulation will be re-enabled during AO2, but this depends on changes to the on-board software. In case the SPI telemetry is continuously overflowing due to background radiation that is higher than expected or due to a strong solar flare, the instrument can be operated in a 'degraded' science mode (TM emergency mode). In this case the onboard

processing and transmission of data will be restricted to 'good' events (non-vetoed), ACS-off energy spectra, and PSD events. The maximum data generation rate in this mode will be about half the rate for normal photon by photon mode. The observer cannot select the TM emergency mode, it is commanded by the ground controllers in case of need.

Before any change of mode the SPI instrument will be put into a special configuration mode. This is the only mode in which changes to the instruments configuration can be made. The instrument will not be taking scientific data when in configuration mode (science telemetry processing is stopped). Several other special modes are available for engineering tasks (e.g. annealing) and for instrument calibrations (e.g. PSD calibration). They are not of interest to the General Observer.

## 3. Dead time

Due to several causes (e.g. veto signals), the SPI instrument experiences within a normal exposure, a dead time, during which no useful scientific data are collected. Experience obtained during AO1 has shown that this dead time is about 12% of the observing time. However, it depends on several external conditions (e.g. increase of the ACS rate during a solar flare). This takes also into account the dead time as a result of ACS vetoes (BGO and plastic scintillator). Another factor which affects the total net science time is the loss of packets as a result of the limited telemetry budget. During most of AO1 an additional 25% of the packets were lost. However, this depends strongly on the allocated telemetry. Since May 2003 the instrument has been operated with a higher telemetry allocation which resulted in no loss of events. This increase in telemetry was possible because the overall INTEGRAL telemetry budget was increased at that time. Since the background count rate has been increasing (approaching Solar minumum) it is expected that during AO3 the deadtime will be around 14%.

## 4. Telemetry budget

In this section the telemetry allocation for the SPI instrument data is discussed. INTEGRAL uses packet telemetry. Each packet corresponds to 0.44 kbps. Experience obtained during A01 revealed that the telemetry needed for the operation of the SPI instrument was higher than expected on the basis of model calculations (mainly due to a higher background than expected). During a large part of AO1 the telemetry budget allocated to SPI has been 69 packets per cycle which resulted in a loss of about 25% of the events. In May 2003 the total available telemetry for INTEGRAL was increased. Since then SPI has been operated with 98 packets per cycle, resulting in basically no loss of events. However, because of the approaching solar minimum and the corresponding increase in the background rate the telemetry allocation for SPI became tight again in mid 2004. In July 2004 the telemetry allocation for SPI was increased by another 5 packets (to 103), which became available because of an optimization of instrument modes for IBIS.

# IV. Using the instrument

## 1. Spectroscopy and timing

In the standard observing mode the instrument can be used for spectroscopy and timing observations. Since every photon is tagged with an accurate time (see section section "Timing capabilities" on page 28 for the timing accuracy), these data can also be used for timing analysis.

It is expected that the background in each of the 19 (17 currently operational) independent detectors will vary in time in a different way. This variation can limit the sensitivity that is obtainable. Several types of background variations can be anticipated:

- short-term variations due to solar activity and solar system "weather".
- variations over the orbital period (related to the position of INTEGRAL in the orbit).
- long-term variations over the mission duration (e.g. solar cycle).

In order to reconstruct the image on the detectors for all pixels in the field-of-view (25 degree field, with 2 degree resolution) for a single pointing a set of 19 (currently 17) equations with 156 unknowns would need to be solved. This is impossible, and the only way to increase the number of equations and make the system solvable is to observe more pointings. Thus, in order to solve this problem of background determination an appropriate dithering strategy has to be adopted for every observation (see also the *"INTEGRAL Manual"*). Dithering is also important to improve the image quality of reconstructed sky images. The dithering strategy that has to be adopted depends on the circumstances:

- observations of a region of multiple or complex sources or of sources with poorly known position. In this case the 5 by 5 rectangular dithering pattern should be used, where 25 points on a rectangular grid with $2^o$ spacing around the source position are observed.
- observation of a single point source of known location, where there are no known other objects of significant intensity in the field-of-view (fully and partially coded, for all dithering points, i.e. within a radius of about $20^o$). In this case the hexagonal dithering pattern can be used, where a hexagonal scan is performed with one pointing centred on the source, surrounded by six pointings with distances of $2^o$. Note that the number of sources for which this dithering pattern can be used is very limited. Experience in AO1 and AO2 has shown that the criteria for hexagonal dither pattern are very seldomly fulfilled and a justification in the proposal for this mode is required. Ususally only when observing a single strong emission line a hexagonal pattern can be justified

Both dithering patterns use a dwell time of 30-60 minutes per point. This range optimised for the instrument performance and expected background variations, while the exact duration is calcu;ated to sample the dither pattern an integral number of times..

All SPI observations should use dithering, since reconstruction for pointed observations is very difficult, if not impossible, due to background inhomogeneities over the detector plane (see above).

The observer should be aware that polarimetry is not supported

## 2. Imaging

The imaging performance of SPI depends also on the dithering pattern that is used. In general the greater the number of pointings, the better the imaging. Calculations were done to estimate the imaging performance of the instrument using simple correlation mapping. More sophisticated techniques may be used to reduce or remove artifacts present in such images, but this can only be done at the expense of worsening the signal to noise ratio or worsening correlations between parts of the image. In these calculations the background in each detector at each energy is assumed to be constant, but different between detectors. The calculations show that, when using the hexagonal dither pattern the reconstructed point source response function shows very strong side lobes at distances of $10^o$ to $20^o$ from the centre. Therefore this mode should only be used for isolated point sources and is not really suitable for imaging. Experience obtained during AO1 has revealed that there are not many isolated point sources (sometimes due to e.g. transients) and observers are in general discouraged to use this mode.The side lobes are still present, but significantly less with the 5 by 5 dither pattern (about 50% of the hexagonal case). To remove these side lobes, which will cause artifacts in reconstructed images, the only possibility is to enlarge the imaged area by observing multiple pointings (i.e. multiple dither patterns). In AO3 a slight modification to the standard 5 by 5 dither pattern will be used: the centre of the dither pattern will move between repetitions of the dither pattern by at most +/- 1.27 degree. Additionally a rotation of the instrument FOV by +/- 3 degree will be applied in a random way. It is expected that these changes to the dither pattern can slightly improve the image reconstruction.

## 3. Gamma-ray burst detection

The ACS system of SPI will detect gamma ray photons from a large part of the sky during all observations. It can thus function as a gamma ray burst monitor. Because of the size of the ACS BGO shield it has a high sensitivity for gamma ray bursts. Experience obtained during the mission shows that the ACS will detect about 2.5 gamma ray bursts per day (minimal detectable energy flux between $4\ 10^{-7}$ erg $cm^{-2}s^{-1}$ and $7\ 10^{-7}$ erg $cm^{-2}s^{-1}$).

Unfortunately the ACS data cannot be directionally sensitive, therefore accurate positions of gamma ray bursts that are detected with the ACS have to be determined through triangulation methods, with other (distant) spacecraft (e.g. Ulysses). About 90 triangulations have been performed at the time of writing. To accommodate these triangulations, the acquisition of the veto count which is done every 50 ms, has a timing error of about 2.5 ms.

The INTEGRAL Science Data Centre (ISDC) will check the stream of veto count rates automatically. If a gamma ray burst is detected (sudden increase in the count rate over a short period of time), an alert will be issued to the institutes that are doing the triangulation observations (4th Interplanetary Network). From the accurate timings of the SPI detection and detections by other spacecraft a position will be constructed that is communicated to the world. The accuracy that can be achieved with this method is much better than an arcminute (due to the long baseline, and the accurate timing of the SPI ACS events). Note that the ACS events are written to the instrument House Keeping and are therefore made public immediately.

Observers can be notified of these gamma ray burst events by subscribing to the gamma ray burst alert system of the INTEGRAL Science Data Centre (see also the INTEGRAL manual).

BGO shield it has a high sensitivity for gamma ray bursts. Experience obtained during AO1 shows that SPI will detect about 2.5 gamma ray bursts per day (minimal detectable energy flux between $4\ 10^{-7}$ erg $cm^{-2}s^{-1}$ and $7\ 10^{-7}$ erg $cm^{-2}s^{-1}$).

Unfortunately the ACS data cannot be directionally sensitive, therefore accurate positions of gamma ray bursts that are detected with the ACS have to be determined through triangulation methods, with other (distant) spacecraft (e.g. Ulysses). To accommodate these triangulations, the acquisition of the veto count which is done every 50 ms, has a timing error of about 2.5 ms.

The INTEGRAL Science Data Centre (ISDC) will check the stream of veto count rates automatically. If a gamma ray burst is detected (sudden increase in the count rate over a short period of time), an alert will be issued to the institutes that are doing the triangulation observations (4th Interplanetary Network). From the accurate timings of the SPI detection and detections by other spacecraft a position will be constructed that is communicated to the world. The accuracy that can be achieved with this method is much better than an arcminute (due to the long baseline, and the accurate timing of the SPI ACS events). Note that the ACS events are written to the instrument House Keeping and are therefore made public immediately.

Observers can be notified of these gamma ray burst events by subscribing to the gamma ray burst alert system of the INTEGRAL Science Data Centre (see also the INTEGRAL manual).GRBs can of course also be detected in the field-of-view of SPI using the normal photon-by-photon mode. In this case the data belongs to the observer who has a accepted proposal for GRBs in the field-of-view (see also the document *"INTEGRAL Science Data Rights"*). A gamma ray burst in the field-of-view occurs about once per month.

# V. Performance of the instrument

## 1. Components and sources of instrumental background

The SPI instrument is background limited. The sensitivity of the instrument is therefore largely dependent on the background and on the correct identification of background photons. The background can be divided into the following main components:

- continuum radiation
- 511 keV line radiation
- gamma ray lines

In the following subsections we will describe each of these components separately.

### 1.1 Continuum background

The continuum background can be split into several components, depending on their origin. First the radiation coming from outside the instrument. This can be the cosmic diffuse gamma ray flux that comes in through the instrument aperture, or leakage through the BGO shield of cosmic diffuse gamma ray radiation and gamma continuum radiation from the spacecraft (induces by energetic cosmic ray particles). Secondly scattering in the Ge detectors of neutrons that were produced in the spacecraft or other parts of the instrument. Thirdly background components produced inside the spectrometer detectors. These consist of localised $\beta^-$ decays, non localised $\beta^-$ decays and $\beta^+$ decays. About 90% of localised $\beta^-$ decays (single events) are identified by the pulse shape discriminator system. The non-localised $\beta^-$ decays (multiple interactions in the detector, e.g. Compton scattering and photoelectric interaction) are more difficult to identify, since in this case the electron and the gamma photon are emitted simultaneously, therefore the resulting pulse looks like a normal 'source' event for the PSD. The continuum emission from the mask and the BGO emission when the veto electronics are blacked out (veto "dead time") are negligible. The individual components and the total continuum background emission are illustrated in Figure 3.

### 1.2 511 keV background

The 511 keV background can be split into four components:

- the continuum background 'under' the 511 keV line. This component is estimated from the continuum background spectrum as explained above.
- passive material: 511 keV photons from passive material, due to $\beta^+$ decays of unstable nuclei in these materials. These unstable nuclei are formed due to interactions of protons and neutrons that are produced in interactions of cosmic ray particles with the detectors, shield or cryostat. The unstable nuclei decay through $\beta^+$ decay. The annihilation of the positron leads to the emission of two 511 keV photons in opposite directions. If one is absorbed by the detector and the other escapes, a 511 keV background event is produced.
- shield leakage: 511 keV photons, originating from interactions of cosmic rays with passive spacecraft materials, that are not rejected by the BGO shield.

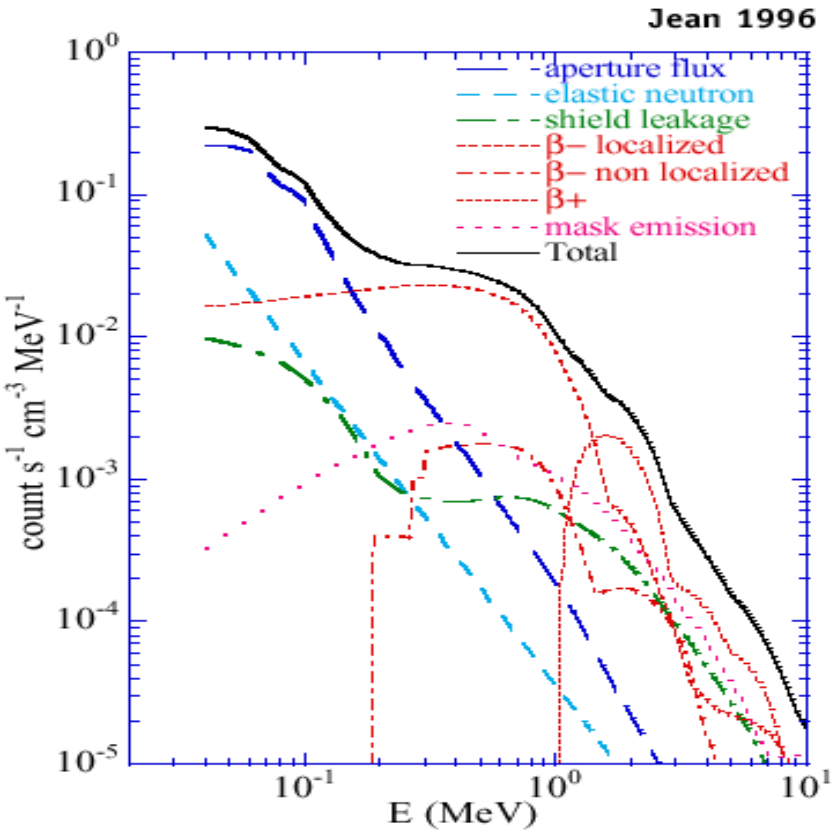


**Figure 3 The continuum background components for SPI. The individual components are identified. The total background spectrum is indicated with the black line. The figure is only indicative:later calculations show a higher total flux above 700 keV.**

- mask component: 511 keV photons originating from cosmic ray interactions with the mask material. The main source is pair creation by cosmic ray proton interactions with W nuclei. This component is reduced by about 8% with the Plastic Scintillator.
- BGO shield blocking time component: 511 keV photons produced by $\beta^+$-decays in the BGO shield when the ACS electronics is blocked by a large energy deposit and the veto is on.

All these components were calculated with a Monte Carlo method.

### 1.3 Background gamma-ray lines

Background gamma-ray lines are emitted in passive materials close to the detectors and in the detector material itself. Primary and secondary cosmic ray particles (protons and neutrons) induce excited nuclei in nuclear reactions with nuclei of the passive material. The prompt or delayed (radioactive) de-excitation of these nuclei leads to gamma-ray lines which can be detected by the germanium detectors. Experience shows that lines originating in the mask do not pose a problem for SPI. In Figure 7 (the narrow-line sensitivity) the background lines can be clearly seen, since they affect the sensitivity.

# 2. Instrumental characterisation and calibration

The SPI instrument has been fully tested and calibrated on ground before the launch. Some tests and calibrations with radioactive sources have been performed on ground with the full satellite. Further testing has been performed during the PV-phase of the mission.The sensitivities, resolution, and other characteristics given in this document are the result of the analysis of the PV-phase observation and other calibration observations. They represent the current best knowledge of the SPI instrumental characterisation.

After launch the SPI team has verfied that the pre-launch calibration, as established on ground, has been maintained. This has been done during the initial in orbit phase (Commissioning Phase) and during an extensive Crab calibration phase in February 2003. Several observations have been performed to measure the imaging performance, spectroscopic performance, background characteristics, flux calibration (sensitivity) and the off-axis response. Currently calibration observations of the Crab nebula and Cygnus X-1 have been used to provide the calibration that will be used for the data processing. The observations of Cygnus X-1 have provided an accurate calibration up to about 2 MeV, confirmed by the Crab observations. Regular observations of the Crab are used to monitor the status of the calibration.

Currently the SPI team and the ISDC are calibrating the instrument using data taken during routine observations. This will allow an accurate determination of e.g. the background. Also lines originating in the BGO shield (511 keV, 6.1 MeV O line) can be used for calibration purposes (e.g. energy calibration), and lines that originate from materials inside the cryostat that have known intensities can be used to measure the Ge detector efficiency. The detector gains, thresholds and resolution versus energy are determined from normal event data and ACS off spectra (for consistency checks) in the routine monitoring task of ISDC. Finally, after every detector annealing (the first one was performed in February 2003) a thorough check has been done of the instrument imaging and spectroscopic response, since these may change as a result of the annealing process. Up to date four annealings have been performed which all increased the resolution. The succes of the annealing depended on the length of the annealing cycle: it was found that about 100 hours of annealing were necessary to restore the full resolution. After the third annealing it was concluded that there was no residual effect of operating in space for more than a year.

Experience obtained during the early mission has also revealed that using the information from the PSD does not significantly increase the signal to noise ratio and is therefore currently not used in the analysis.

# 3. Measured performance

## 3.1 Imaging resolution

The measured angular resolution for (isolated) point sources is about $2.5^{o}$ (FWHM).This is the measured width of the instrument response correlation for a point source. The location of point sources can be done with an accuracy better than this, but this depends on the strength of the source. As explained above, dithering is required for SPI, especially for regions with more than

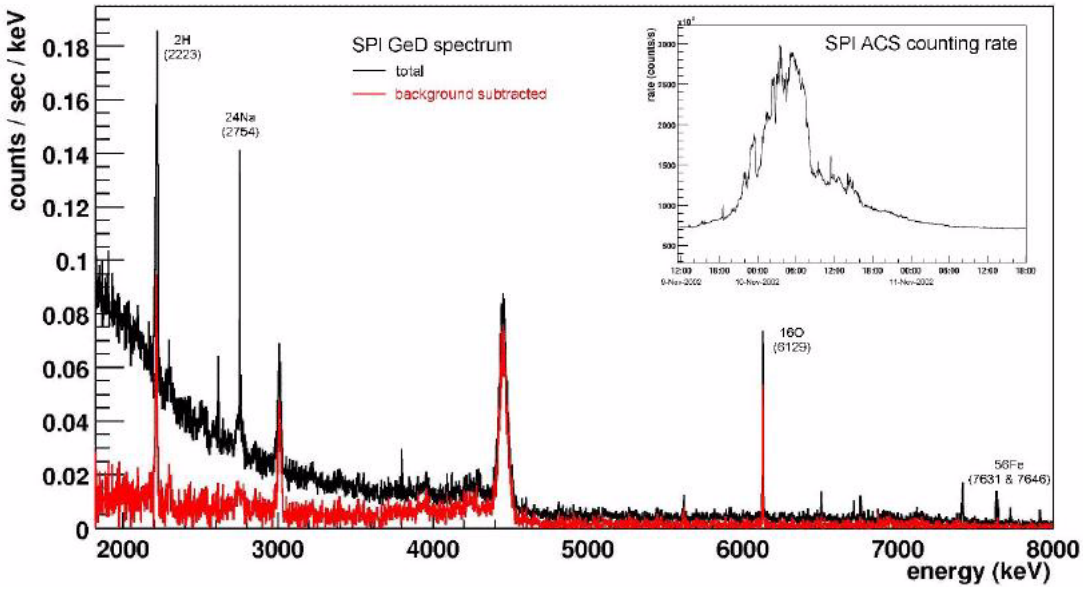


**Figure 4 Example spectrum taken during a solar flare (see inset in top-right), indicating the ability to resolve lines.**

one source or diffuse emission. Positions obtained from SPI have an uncertainty, which is mainly statistical and therefore countrate dependent. The uncertainties decrease as the inverse of the detection significance, and range from ~10-~1 arc minute for detection significances of ~10 to ~100. For higher detection significances (e.g. the Crab) the detection is ultimately limited to ~0.5 arcmin in position.

### 3.2 Spectral resolution

The spectral resolution has been measured in the laboratory with detectors that are representative of the flight units, and afterwards with flight model detectors and pre amplifiers. An example spectrum measured inflight is shown in Figure 4. The measured energy resolution as a function of energy for an individual detector is given in Figure 5. The energy resolution for the full instrument is given in Table 2. The energy resolution does not depend strongly on the temperature of the detectors, therefore even in the case of a failure of one of the coolers, the spectroscopic capability of the instrument is not significantly degraded. However small variations in energy are observed over and between orbits, partly a function of temperature. Therefore calibrations are routinely performed on a per-orbit time base, and for fine spectroscopy re-calibrations may be required.

The energy resolution also slowly degrades as a function of time by about 20% in 6 months as a result of radiation damage in the Ge crystals induced by cosmic particles. The damage is not permanent and can be corrected by the annealing procedure, which is foreseen to take place about

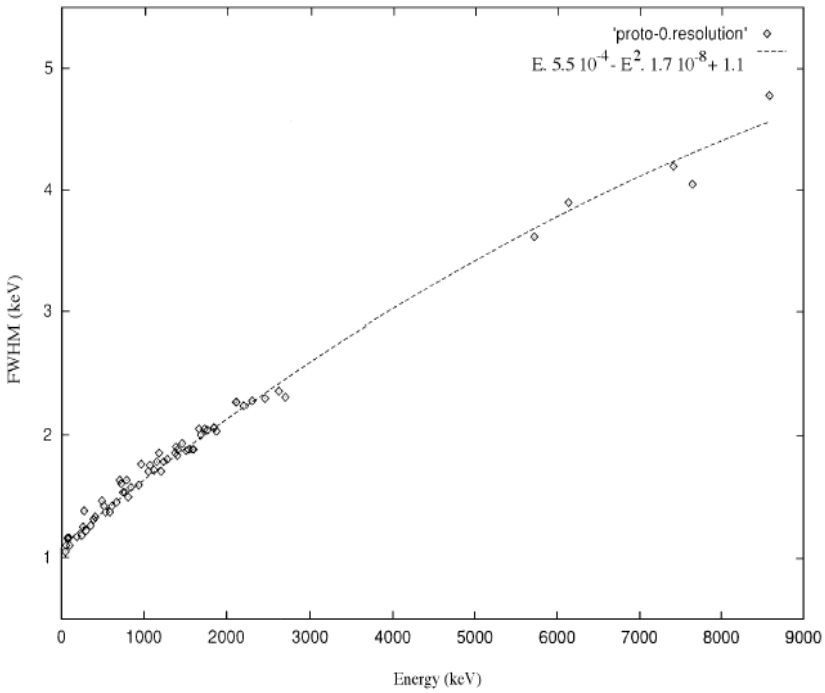


**Figure 5 The measured energy resolution of an individual SPI detector. This was measured using laboratory detectors. The resolution of the full instrument with all 19 detectors is slightly lower than this.**

every 6 months. Annealings have been performed in February 2003, July 2003, November 2003 and June 2004. The evolution of the resolution can be seen in Figure 9.

The energy calibration has been determined by fitting the some (well-suited) background lines. The obtained absolute precision of the energy calibration is about 0.1 keV in the 500 keV to MeV range, while a relative accuracy of 0.01-0.02 keV can be reached. The continuum and line sensitivities of the SPI instrument are given in Figure 6 and Figure 7. In Table 2 the instrument performance numbers (energy resolution, continuum and line sensitivities) are given at a number of energies in the SPI range. The sensitivities given in this table are 3 sigma in $10^6$ seconds pure integration time, using a BGO threshold of 80 keV, a plastic scintillator threshold of 300 keV, and with PSD and multiple event reduction techniques applied (this is similar to the normal operating mode). The continuum sensitivities are for ΔE=E/2, and are calculated from the narrow line sensitivity by dividing those by $\sqrt{R \cdot \Delta E}$ where R is the instrument resolution for lines. The line sensitivities are fluxes in photons $cm^{-2}$ $s^{-1}$, the continuum sensitivities are fluxes in photons $cm^{-2}$ $s^{-1}$ $keV^{-1}$. The line sensitivities are for narrow lines. For broad lines, the sensitivity of the instrument degrades, as can be seen in Figure 8, where the factor is plotted with which the sensitivity is degraded as function of the energy for three line widths (1, 3 and 10% of the energy of the line). Note that the 511 keV sensitivity is worse than the surrounding continuum due to the strong 511 keV background line originating in the instrument.

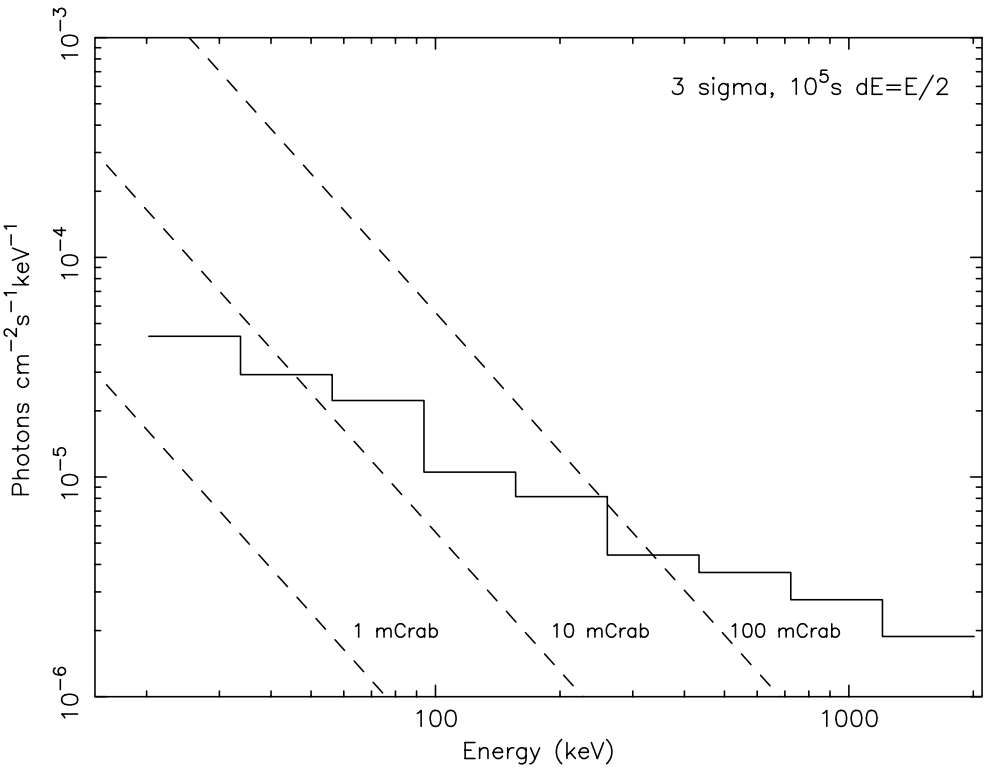


**Figure 6 The continuum sensitivity of the SPI instrument for a 3 sigma detection in $10^5$ seconds on-axis. Fluxes are for E=E/2. The dashed lines indicate extrapolation from X-rays using a powerlaw with photon index -2.1 for 1, 10,,and 100 mCrab.**

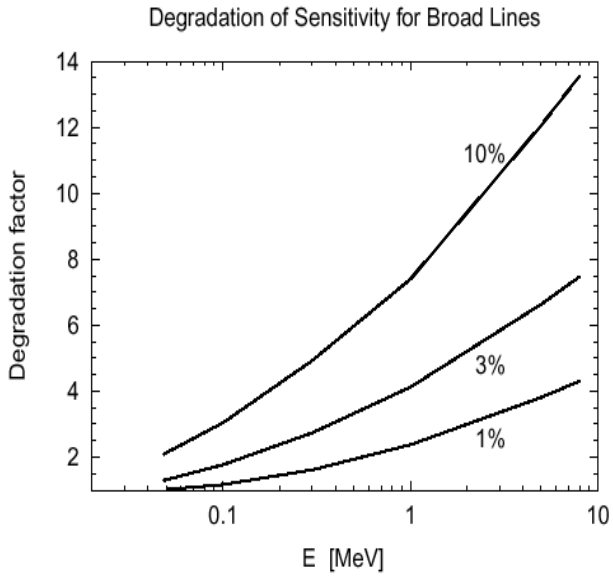


**Figure 8 The degradation factor of the line sensitivity for broad lines (with a width of 1, 3 and 10% of the line energy) as a function of energy.**

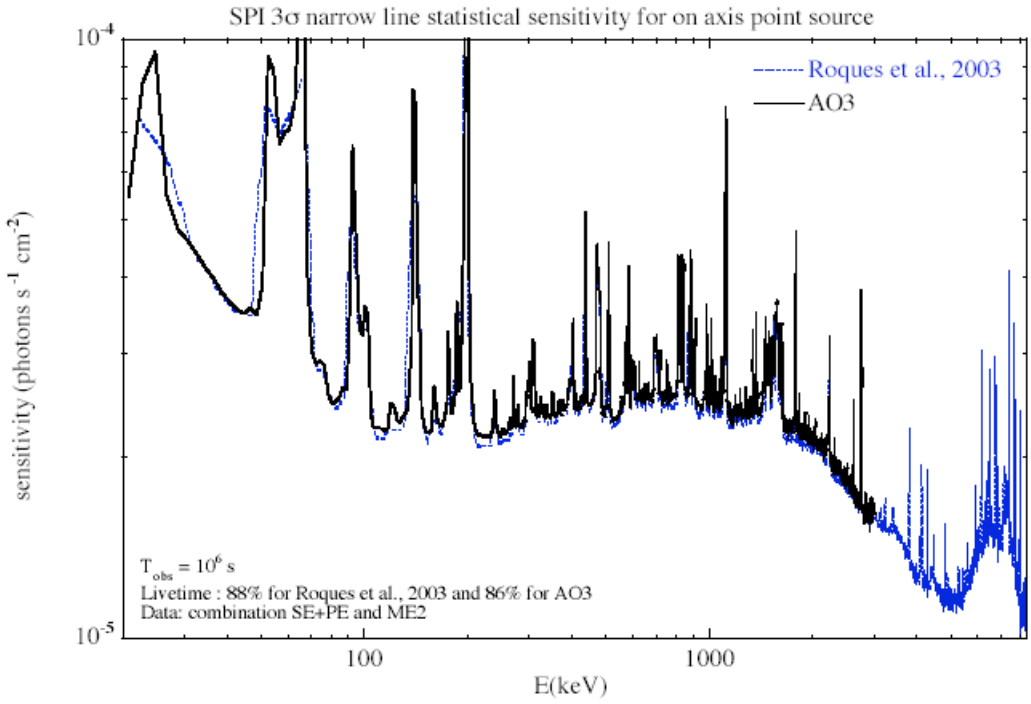


**Figure 7 The narrow line (w.r.t. the instrument resolution) sensitivity of the SPI instrument for a 3 sigma detection in $10^6$ seconds.**

**Table 2 The energy resolution (FWHM), narrow line and continuum sensitivities of the SPI instrument. (3 sigma detection in $10^6$ seconds) Note that the line sensitivities can be a very strong function of energy close to the lines. See Figure 7.**

| Energy (keV) | Resolution (keV) | Continuum sensitivity (ph $cm^{-2}s^{-1}keV^{-1}$) | Line sensitivity (ph $cm^{-2}$ $s^{-1}$) |
|---|---|---|---|
| 50 | 1.531 | $9.2\ 10^{-6}$ | $5.6\ 10^{-5}$ |
| 100 | 1.563 | $3.3\ 10^{-6}$ | $3.3\ 10^{-5}$ |
| 200 | 1.654 | $2.6\ 10^{-6}$ | $3.1\ 10^{-5}$ |
| 300 | 1.76 | $1.4\ 10^{-6}$ | $2.5\ 10^{-5}$ |
| 400 | 1.85 | $1.410^{-6}$ | $2.8\ 10^{-5}$ |
| 500 | 1.926 | $1.2\ 10^{-6}$ | $2.3\ 10^{-5}$ |
| 511 | 1.933 | $1.2\ 10^{-6}$ | $4.6\ 10^{-5}$ |
| 600 | 1.992 | $1.2\ 10^{-6}$ | $2.6\ 10^{-5}$ |
| 700 | 2.051 | $1.2\ 10^{-6}$ | $3.0\ 10^{-5}$ |
| 800 | 2.106 | $8.8\ 10^{-7}$ | $2.5\ 10^{-5}$ |
| 900 | 2.158 | $8.8\ 10^{-7}$ | $2.7\ 10^{-5}$ |
| 1000 | 2.209 | $8.8\ 10^{-7}$ | $2.4\ 10^{-5}$ |
| 1100 | 2.257 | $8.8\ 10^{-7}$ | $2.5\ 10^{-5}$ |
| 1200 | 2.303 | $8.8\ 10^{-7}$ | $2.3\ 10^{-5}$ |
| 1300 | 2.347 | $5.9\ 10^{-7}$ | $2.3\ 10^{-5}$ |
| 1400 | 2.389 | $5.9\ 10^{-7}$ | $2.3\ 10^{-5}$ |
| 1500 | 2.432 | $5.9\ 10^{-7}$ | $2.7\ 10^{-5}$ |
| 1600 | 2.473 | $5.9\ 10^{-7}$ | $2.5\ 10^{-5}$ |
| 1700 | 2.513 | $5.9\ 10^{-7}$ | $2.1\ 10^{-5}$ |
| 1800 | 2.553 | $5.9\ 10^{-7}$ | $2.1\ 10^{-5}$ |
| 1900 | 2.593 | $5.9\ 10^{-7}$ | $2.2\ 10^{-5}$ |
| 2000 | 2.634 | $5.9\ 10^{-7}$ | $2.0\ 10^{-5}$ |
| 2250 | 2.73 | $2.8\ 10^{-7}$ | $1.9\ 10^{-5}$ |
| 2500 | 2.821 | $2.8\ 10^{-7}$ | $1.8\ 10^{-5}$ |
| 3000 | 2.997 | $2.8\ 10^{-7}$ | $1.6\ 10^{-5}$ |
| 3500 | 3.162 | $1.4\ 10^{-7}$ | $1.5\ 10^{-5}$ |
| 4000 | 3.32 | $1.4\ 10^{-7}$ | $1.3\ 10^{-5}$ |
| 4500 | 3.471 | $1.4\ 10^{-7}$ | $1.2\ 10^{-5}$ |
| 5000 | 3.616 | $1.4\ 10^{-7}$ | $1.1\ 10^{-5}$ |
| 5500 | 3.757 | $1.4\ 10^{-7}$ | $1.2\ 10^{-5}$ |
| 6000 | 3.889 | $1.2\ 10^{-7}$ | $1.5\ 10^{-5}$ |
| 6500 | 4.018 | $1.2\ 10^{-7}$ | $1.710^{-5}$ |
| 7500 | 4.26 | $1.2\ 10^{-7}$ | $1.5\ 10^{-5}$ |
| 8000 | 4.376 | $1.2\ 10^{-7}$ | $1.1\ 10^{-5}$ |

**Table 3 Energy resolution for various lines after (third) annealing and before (fourth) annealing.**

| Line (keV) | Events | After third annealing | Before fourth annealing |
|---|---|---|---|
| 174.95 | ME | 1.82 | 1.91 |
| 198.4 | SUM | 1.84 | 1.95 |
| 264.6 | ME | 1.87 | 1.96 |
| 309.9 | SUM | 1.90 | 2.03 |
| 584.6 | SUM | 2.06 | 2.24 |
| 1368.6 | SUM | 2.49 | 2.91 |
| 1764.3 | SUM | 2.78 | 3.37 |
| 2754 | SUM | 3.89 | 5.16 |

In December 2004 detector #2 stopped working and all attempts to revive the detector have failed. This detector is now considered to be dead permanently. The failure of this detector has a slight impact on the sensitivities for continuum and background, which are taken into account in the figures presented here. The impact on sensitivity is only very small (about 2% for the continuum), since the countrates of single events in neigbouring detectors has increased (since double events have now become single events). Only the sensitivity for the 511 keV line has been reduced by 5-10%, because of the loss of information in the multiple events Recently (on July 17 2004) detector 17 also failed. The impact on the sensitivity has not been included in the figures presented here, but should be in the same range.

The tabulated sensitivities above 2 MeV in Table 2 are older values taken from the Roques et al. (2003; A&A 411, L91) paper, which match the more recent data below 2 MeV very well.

### 3.3 Dithering sensitivity degradation

The instrumental sensitivities given in Table 2 and Figure 6 and Figure 7 are for a source on axis, and do not take into account dithering. As stated earlier (see section "Spectroscopy and timing" on page 14 ), observations with SPI should not be done in staring mode, since this makes the identification and removal of the background impossible. Dithering on the other hand has the disadvantage that the source is not observed for the full integration time in the centre of the fully coded filed of view (centre of the instrument response). The SPI response falls off towards the edge of the filed of view, and therefore dithering will degrade the sensitivity of the instrument somewhat. The hexagonal dither (a central pointing with six surrounding pointings in hexagonal pattern, all $2^o$ apart) only samples the central part of the SPI fully coded field-of-view. Therefore no reduction in the sensitivity is noticable. The 5 by 5 dither (a square pattern of 5 by 5 pointings around the source, all with $2^o$ spacing) however samples closer to the edge of the fully coded

field-of-view. In this case the sensitivity is degraded by a factor 0.8374 (i.e. the sensitivities given in Table 2 should be divided by this number to get the effective sensitivity).

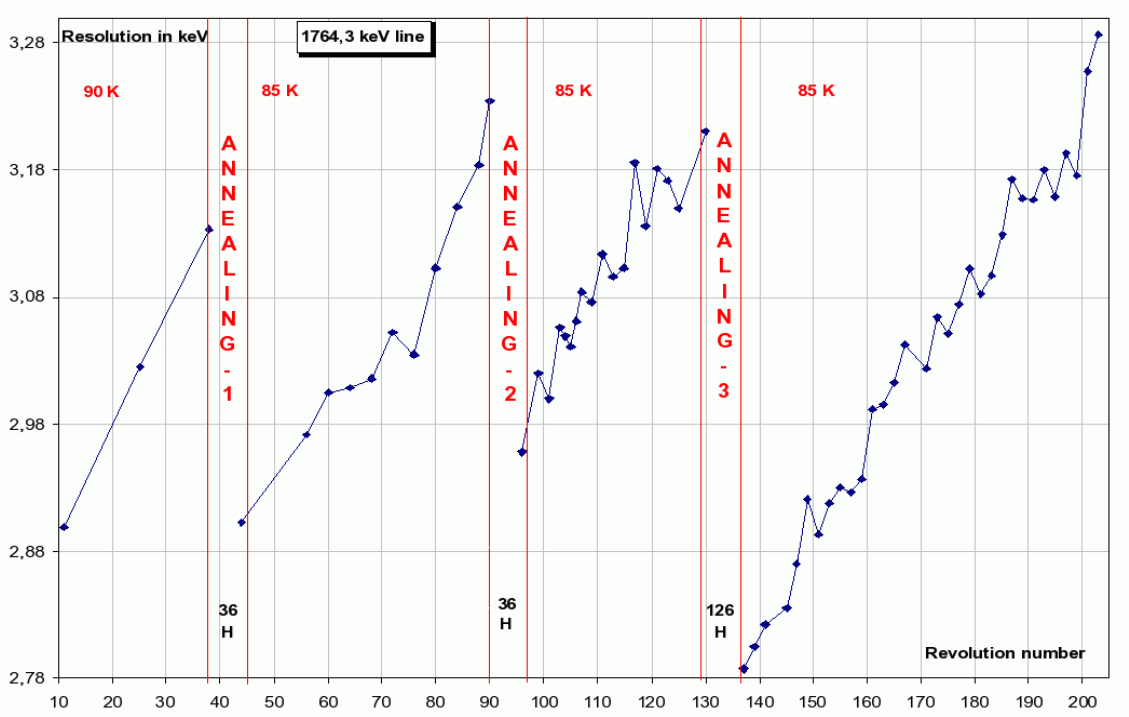


**Figure 9 The evolution of energy resolution as a function of time in-between the annealing periods.**

### 3.4 Detection of off-axis sources

The wide field-of-view of SPI allows the detection of off-axis sources. However it also means that off-axis sources will create a shadowgram on the detector that increases the background photons for the prime target. To remove this 'background' a proper mapping of the source and the surroundings is necessary. This is the main reason why hexagonal dithering should only be used for isolated point sources, where no significant contribution is expected from other sources within about $20^{o}$. In order to allow the observer to estimate the significance of an off-axis detection, we give the reduction factor for the sensitivity for hexagonal and 5 by 5 dithers in Table 4. The reduction for staring is similar to the one for hexagonal dithers. Observers can calculate the effective sensitivity by dividing the sensitivity limits given in Table 2 by the factor given in Table 4.

### 3.5 Imaging capabilities

The values presented in Table 2 are for an identified point source (i.e. a 3σ excess in a pixel). However for unknown sources in an image of an area of sky, the situation is slightly different. In a map containing a large number of pixels, the probability that an n-sigma excess will occur by chance somewhere in the map can be significantly higher than suggested by the integral error function. In a SPI map covering, say 25x25 degrees there are approximately 60 independent pixels. Thus 99% confidence that a source at a specific position (a "known" source) is real requires 2.35 sigma, whereas 99% confidence that a source found at an arbitrary position somewhere in the field (an new "unknown" source) is real requires 3.6 sigma significance. Therefore to identify

new, unknown sources in the field-of-view, a higher significance is required than for an known source in the field-of-view (since probability for an chance n-sigma excess due to noise somewhere in the map is higher).

**Table 4 Sensitivity degradation factor as function of the distance off-axis for a hexagonal and a 5 by 5 dither pattern.**

| Off axis distance (degrees) | Sensitivity degradation | |
|---|---|---|
| | hexagonal | 5 by 5 |
| 0 | 1.0 | 0.8374 |
| 1 | 0.6655 | 0.7925 |
| 2 | 0.7638 | 0.8004 |
| 3 | 0.6838 | 0.7879 |
| 4 | 0.7147 | 0.7874 |
| 5 | 0.7056 | 0.7746 |
| 7.5 | 0.6309 | 0.7357 |
| 10 | 0.5505 | 0.6718 |
| 12.5 | 0.4938 | 0.5918 |
| 15 | 0.3749 | 0.5002 |
| 17.5 | 0.1888 | 0.3774 |
| 20 | 0.0886 | 0.2047 |
| 25 | 0.0 | 0.0148 |
| 30 | 0.0 | 0.0 |

### 3.6 Timing capabilities

The instrument works in photon by photon mode. Each photon data set includes timing information given by a 100 μs clock signal. This clock is synchronised to the on board clock, and thus to the UTC. The timing error budget for SPI is derived from:

- the accuracy of the onboard clock and the synchronisation,
- the conversion between onboard time and UTC,
- the conversion between UTC arrival time at the spacecraft and the arrival time at the solar system barycentre.

The resulting SPI timing accuracy calculated in this way is 129 μs, 3σ accuracy, and a 90% confidence accuracy of 94 μs. A timing analysis of the Crab data has revealed that the absolute timing accuracy is about 40 μs (1σ uncertainty).

However, due to strict limits on the telemetry allocation, the SPI instrument has been operated during a large part of AO1 in a mode where the Single Event photons are only downloaded as part of the histograms, this severely degrading the time resolution for these events to 30 minutes. The increased telemetry budget for SPI allowed to restore the original time resolution for single events. A software patch has been prepared to apply background line filtering onboard and

a more efficient coding of events which will provide sufficient margin to the SPI telemetry needs towards solar minimum when an increase of the background is expected

# VI. Observation "Cook book"

## 1. Astronomical considerations on the use of the instrument

The SPI instrument is designed as a spectrometer, therefore it should primarily be used for high resolution spectroscopy on sources with (narrow) lines, possibly on top of a continuum. Given the imaging qualities of the instrument it can also be used for wide field imaging of diffuse emission, especially in (narrow) emission lines. However if high resolution imaging, or observations of sources with only continuum emission or very broad lines are needed, the IBIS instrument might be better suited as prime instrument, at least below a few hundred keV.

The prime astrophysical topics to be addressed with SPI are nucleosynthesis processes, supernova theories, nova theories, interstellar physics and pair plasma physics in compact objects (neutron stars, black holes). A number of interesting lines fall in the SPI energy range. Table 5 gives a list of some lines and energies.

**Table 5 Some gamma ray lines from cosmic radioactivity in the SPI energy range.**

| isotope | decay chain | line energies (MeV) | Mean life (year) |
|---|---|---|---|
| $e^+$ | $e^+ + e^- \rightarrow$ photon | 0.511 | ~1 $10^5$ |
| $^{56}$Co | ($^{56}$Ni) $\rightarrow$ $^{56}$Co $\rightarrow$ $^{56}$Fe | 0.847 1.238 | 0.31 |
| $^{22}$Na | $^{22}$Na $\rightarrow$ $^{22}$Ne | 1.275 | 3.8 |
| $^{44}$Ti | $^{44}$Ti $\rightarrow$ $^{44}$Sc $\rightarrow$ $^{44}$Ca | 1.156 | 89 |
| $^{26}$Al | $^{26}$Al $\rightarrow$ $^{26}$Mg | 1.809 | 1.0 $10^6$ |
| $^{60}$Fe | $^{60}$Fe $\rightarrow$ $^{60}$Co $\rightarrow$ $^{60}$Ni | 1.173 1.322 | 2.2 $10^6$ |

## 2. How to estimate observing times

The formal way to calculate accurate observing times is via the Observing Time Estimator (OTE). OTE can be found on http://www.rssd..esa.int/Integral/isoc/operations/html/OTE.html. In this section however we give an easy way for observers to estimate the observing times using simple formulae. The times that are calculated in this way are reasonably accurate, and are for most cases within a few percent from the OTE calculated times. In the worked examples we give both times for comparison. Note that the ISOC will only use the OTE to assess the technical feasibility of proposals.

General observers can request to observe a gamma-ray line flux (in photons $cm^{-2}s^{-1}$) or an integrated continuum flux over an energy band (also in photons $cm^{-2}s^{-1}$) at a given energy from a point source.Therefore, two types of observation time calculation will be presented in the following sections. The continuum sensitivity can be estimated using the narrow line sensitivity, the energy resolution and the energy-band required. In the Proposal Generation Tools, PGT, a line has to be given in as a narrow energy range with the width of the line. The inputs to both OTE and PGT for continuum are for an in-band flux, and since the sensitivities are for ΔE=E/2, the band over which the flux is specified should not be too broad (maximum ΔE=E/2) to perform calculations. However, with the latest version of OTE one can specify a power-law slope and OTE will split the total energy band up into many small bands and combine the results. The observers should make sure that observing times entered into PGT allow the completion of at least one full dither pattern (i.e. minimum of 12600 seconds for hexagonal dithers and 45000 seconds for 5 by 5 dithers).

### 2.1 Gamma-ray line

The observation time, $T_{obs}$ (in kilo seconds), is estimated using the relation

$$T_{obs} = 1 \cdot 10^3 \left( \frac{N_\sigma}{3} \cdot \frac{S_{line}}{F_{line} \cdot Frac} \right)^2 \cdot \frac{\Delta E}{R} \cdot \frac{1}{1 - f_{dead}}$$

where:

- $N_\sigma$ is the number of sigma required.
- $S_{line}$ is the 3σ, point source on-axis, narrow line sensitivity for SPI at the considered energy and for $10^6$ s and a lifetime of 100%. The values of this parameter are in Table 2.
- $F_{line}$ is the source line flux in ph/s $cm^2$.
- *Frac* is the sensitivity degradation factor due to the dithering or the source being off-axis. See section "Dithering sensitivity degradation" on page 25 and section "Detection of off-axis sources" on page 26 for details.
- $\Delta E$ is the width of the expected gamma-ray line (FWHM in keV).
- $R$ is the energy resolution of the spectrometer (in keV). It depends on the energy, the values of this parameter are in Table 2.
- $f_{dead}$ is the fraction of dead-time (12%). This parameter is described in section "Dead time" on page 13 .

### 2.2 Gamma-ray continuum

The observation time, $T_{obs}$ (in kilo seconds), is estimated using the relation:

$$T_{obs} = 1 \cdot 10^3 \left( \frac{N_\sigma}{3} \cdot \frac{S_{line}}{F_{int} \cdot Frac} \right)^2 \cdot \frac{\Delta E}{1.5R} \cdot \frac{1}{1 - f_{dead}}$$

$$= 1 \cdot 10^3 \left( \frac{N_\sigma}{3} \cdot \frac{S_{cont}}{F_{cont} \cdot Frac} \right)^2 \cdot \frac{E}{2\Delta E} \cdot \frac{1}{1 - f_{dead}}$$

Where:

- $F_{int}$ is the flux integrated over the specified band (in ph/$cm^2$s)
- $F_{cont}$ is the continuum flux in the specified band (in ph/$cm^2$s keV)
- $\Delta E$ is the width of the energy band corresponding to the specified flux (in keV)

- $S_{cont}$ is the continuum sensitivity as given in Table 2. The continuum sensitivity can be calculated from the line sensitivity using: $S_{cont} = S_{line}/(\sqrt{1.5R \cdot \Delta E})$

All other parameters are as described above. The factor 1.5 is used to correct the gamma-ray line sensitivity that is calculated assuming that the total counts in a line are contained in an energy band of 1.5 times the spectral resolution (FWHM). Actually, 1.5 times the resolution contains ~95% of the line counts..

## 3. Worked examples

In this section we present some examples of observations with SPI for which we calculated the observing times with the formulae given above and the Observing Time Estimator. Note that for lines, the exposure time derived from OTE differs from the one calculated from the formula. This is because OTE uses sensitivities at a much higher energy resolution than tabulated in Table 2 (see Figure 7). The examples below (for lines) are therefore only intended as an order of magnitude estimate; one should use the exposure times obtained with OTE.

- **Example 1**: a line at 1809 keV ($^{26}$Al), with a 3 keV width, and a integrated line flux of $5 \cdot 10^{-5}$ ph cm$^{-2}$s$^{-1}$, observed with a 5 by 5 dither pattern. The requested significance is 3 sigma. The sensitivity at this energy is 2.1 $10^{-5}$ ph cm$^{-2}$s$^{-1}$, the resolution is 2.553 keV, and the sensitivity degradation factor for a 5 by 5 dither is 0.8374. Using these numbers the required observing time would be 224 ksec or 2.59 days (OTE gives 493 ksec).
- **Example 1a**: (to show the correspondence between manual and OTE results at an energy where the line sensitivity is fairly constant) a line at 2000 keV, with a 3 keV width, and a integrated line flux of $5 \cdot 10^{-5}$ ph cm$^{-2}$s$^{-1}$, observed with a 5 by 5 dither pattern. The requested significance is 3 sigma. The sensitivity at this energy is 2.0 $10^{-5}$ ph cm$^{-2}$s$^{-1}$, the resolution is 2.634 keV, and the sensitivity degradation factor for a 5 by 5 dither is 0.8374. Using these numbers the required observing time would be 295 ksec or 3.41 days (OTE gives 337 ksec).
- **Example 2**: the same 1809 keV line, but now observed with a hexagonal dither (sensitivity degradation factor 1.0) would for a significance of 3 sigma require 157 ksec, or 1.82 days (however, this mode is only applicable for isolated point sources) (OTE gives 283 ksec).
- **Example 3**: a continuum band of 150 keV width, centred at 350 keV, with a continuum flux of 2 $10^{-5}$ ph cm$^{-2}$s$^{-1}$keV$^{-1}$, observed with a 5 by 5 dither for significance of 10 sigma. The continuum sensitivity for this energy is 1.4 $10^{-6}$ ph cm$^{-2}$s$^{-1}$keV$^{-1}$, the resolution is 1.80 keV and the sensitivity degradation factor is again 0.8374. This observation would then require 103 ksec, or 1.19 days (OTE gives 102 ksec with an in-band flux of 3.0 $10^{-3}$ ph cm$^{-2}$s$^{-1}$).
- **Example 4**: the $^{44}$Ti line (at 1.160 MeV) in a supernova remnant (e.g. Cas A). The line width is 2000 km/sec (or 7.73 keV), the integrated line flux 1 $10^{-4}$ ph cm$^{-2}$s$^{-1}$. The source should be observed with a 5 by 5 dither, for a significance of 5 sigma. The sensitivity of the instrument at this energy is 2.4 $10^{-5}$ ph cm$^{-2}$s$^{-1}$, the resolution is 2.28 keV, and the sensitivity degradation factor is again 0.8374. The required observing time for a significance of 5 sigma would then be 586 ksec or 6.78 days (OTE gives 861 ksec).
- **Example 5**: a broad, red shifted 511 keV line. The energy of the line is 470 keV, with a width of 5000 km/sec (or 16 keV), and a integrated line flux of 3.3 $10^{-4}$ ph cm$^{-2}$s$^{-1}$. The observation should be in hexagonal dithering mode (isolated source), for a significance of 5 sigma. The sensitivity of the instrument at this energy is 4.6 $10^{-5}$ ph cm$^{-2}$s$^{-1}$, the energy resolution is

1.93 keV and the sensitivity degradation factor is 1.0. This observation would then take 347 ksec, or 4.02 days (OTE gives 274 ksec).

- **Example 6**: a continuum band of 500 keV width, centred at 4 MeV, with a continuum flux of 1 $10^{-6}$ ph $cm^{-2}s^{-1}keV^{-1}$. The observation should using a 5 by 5 dither pattern, and should achieve 3 sigma on source. The sensitivity of the instrument is 1.4 $10^{-7}$ ph $cm^{-2}s^{-1}keV^{-1}$, the resolution is 3.32 keV and the sensitivity degradation factor is 0.8374. This observation would require 172 ksec, or 2.0 days (OTE gives 698 ksec, assuming a constant photonflux over the energy band, giving an in-band flux of 5 $10^{-4}$ ph $cm^{-2}s^{-1}$).
- **Example 7**: an extended source with a size of 4.8 arc minutes and a continuum flux in a band of 150 keV centered at 350 keV of 2 $10^{-5}$ ph $cm^{-2}s^{-1}$ $keV^{-1}$. With an angular resolution of 2.5 degrees, the source can be resolved in $(4.8/2.5)^2$ pixels. In 102 ks a sensitivity of 10/(4.8/2.5) (see example 3) or 5.2 sigma can be reached

# Index

**A**
Anti-coincidence system 5–7, 10–13, 15, 19

**B**
background . . . . . 6, 10, 12–15, 17–19
511 keV . . . . . 10, 17
continuum . . . . . 17–18
BGO . . . . . 6, 10, 13, 15, 17, 19, 21

**C**
calibration . . . . . 13, 19
Compton Gamma Ray Observatory . . . . . 5
cryostat . . . . . 5, 8–9, 17, 19

**D**
dead time . . . . . 11, 13
detector . . . . . 5–6, 8–12, 14–15, 17, 19–21
dither . . . . . 12, 14–15, 19, 25, 28, 32
5 by 5 . . . . . 12, 14–15, 28, 32
hexagonal . . . . . 12, 14–15, 28, 32

**E**
electronics . . . . . 5, 9–12, 17
example . . . . . 20, 31

**G**
gamma-ray burst . . . . . 16
gamma-ray continuum . . . . . 31
gamma-ray line . . . . . 31

**I**
imaging . . . . . .5, 7, 12, 15, 19, 30

**M**
mask . . . . . .6–8, 10, 12, 17–18
modes . . . . . .12–13

**O**
observing times . . . . . .29, 32
off-axis . . . . . .28, 31

**P**
plastic scintillator . . .6–7, 10, 12–13, 18, 21
pre-amplifier . . . . . .9, 20
pulse shape discriminator 5–6, 9, 11–13, 17, 21

**S**
sensitivity
continuum . . . . . .24, 30–32
line . . . . . .21–24, 30–32
spectral resolution . . . . . .20, 31
spectroscopy . . . . . .5, 12, 14, 30

**T**
telemetry . . . . . .11–13
timing . . . . . .14–15, 28
accuracy . . . . . .14, 28

**V**
veto . . . . . .6, 9–13, 15, 17